eprints@whiterose.ac.uk
https://eprints.whiterose.ac.uk/

How memory of direct animal interactions can lead to territorial pattern formation

Jonathan R. Potts[1,a], Mark A. Lewis[2,3]

Key words: Mathematical ecology, Partial differential equations, Pattern formation, Ritualised aggression, Territoriality

1 School of Mathematics and Statistics, University of Sheffield, UK
2 Centre for Mathematical Biology, Department of Mathematical and Statistical Sciences, 632 CAB, University of Alberta, Canada, T6G 2G1.
3 Department of Biological Sciences, University of Alberta, Edmonton, Canada
a E-mail: j.potts@sheffield.ac.uk. Phone: +44(0)114-222-3729.

Abstract

Mechanistic home range analysis (MHRA) is a highly effective tool for understanding spacing patterns of animal populations. It has hitherto focused on populations where animals defend their territories by communicating indirectly, e.g. via scent marks. However, many animal populations defend their territories using direct interactions such as ritualised aggression. To enable application of MHRA to such populations, we construct a model of direct territorial interactions, using linear stability analysis and energy methods to understand when territorial patterns may form. We show that spatial memory of past interactions is vital for pattern formation, as is memory of 'safe' places, where the animal has visited but not suffered recent territorial encounters. Additionally, the spatial range over which animals make decisions to move is key to understanding the size and shape of their resulting territories. Analysis using energy methods, on a simplified version of our system, shows that stability in the non-linear system corresponds well to predictions of linear analysis. We also uncover a hysteresis in the process of territory formation, so that formation may depend crucially on initial space-use. Our analysis, in 1D and 2D, provides mathematical groundwork required for extending MHRA to situations where territories are defended by direct encounters.

1 Introduction

Territorial conflicts occur in many different animal species, from birds to primates, insects to reptiles [1–4]. They sometimes take the form of physical fights, e.g. for monkeys [5] and humans [6, 7]. However, to avoid costly injuries, animals often eschew fighting in favour of 'ritualised aggression', expressing dominance through displays, vocalisations, and other non-violent interactions [8]. For example, ritualised aggression has been observed in many bird species, where plumages have often evolved to aid in displays of territorial dominance [9–11]. Likewise, bees have been observed to perform 'perching and patrolling' displays to highlight their territories [3]. In some cases, the line between non-violent and violent can become blurred, when ritualised displays turn into violent encounters (e.g. [2]). Nonetheless, be they violent or ritualised, the aim of territorial conflicts is to gain and defend parts of space for exclusive use by a select subset of the population, such as a flock, pack, tribe, nation, or mating pair. Although aggressive interactions are sometimes non-territorial, here we focus on those that are, so may result in patterns of spatial segregation: interlocking territories that remain relatively stationary over time [12].

In this paper, we show mathematically how the process of territorial conflicts may give rise to spatial segregation patterns, and under what conditions these patterns may emerge or break down. This builds upon an established body of work on territorial pattern formation and home range analysis in scent-marking animals [13–15], which has been fruitful for accurate capture of home range patterns [16], predicting changes in territorial structure [17–19], and uncovering environmental drivers of spatial patterns [19, 20]. However, such 'mechanistic home range analysis' (MHRA) studies all rely on there being a process of *indirect* interaction, whereby individuals mark the area throughout their terrain and then other individuals react to those marks. As noted in recent reviews [14, 21], this constraint greatly limits the potential use of MHRA, as many populations instead use combats or ritualised aggression for territorial defence.

Here, we remedy this shortcoming by focusing on *direct* interactions (which we term 'con-

flicts'), which of necessity can only occur at points on the borders between territories. Indeed, although MHRA has been used for understanding spatial structures of human gangs [4], where graffiti marking is used as a proxy for scent marking, that study also noted that direct confrontations between gangs may be influential in determining spatial structure. Similarly, the study of [22] demonstrated that memory of neighbouring vocalisations in bird populations may be modelled in an analogous way to scent-marking in canid populations. Yet, those bird populations are also known to engage in ritualised aggression for the purposes of territorial defense [23]. Therefore both [4] and [22] would be improved by mechanistic models of direct territorial interactions. In general, by bringing direct interaction processes into the framework of MHRA [13, 14], this paper expands the range of possible species and populations that may be studied using MHRA.

2 The Model

We begin with some terminology, not intended to be definitive, but introduced purely for the purposes of this paper. Animals may move by themselves or as clusters of individuals (e.g. a pack or a flock), so we use the term 'agent' to mean either a lone-moving individual, or a cluster of individuals moving together. By 'territorial conflict' we mean any direct interaction that seeks to exclude certain agents from an area of space. For example, a territorial conflict could mean a physical fight, or a display of ritualised aggression.

To perform mathematical analysis, we start by describing a model of two agents living on a line segment. This analysis allows us to gain a rigorous understanding of the conditions under which territories can form. This understanding is then carried over into the more realistic 2D situation, where we perform simulation analysis to provide evidence that our model can give rise to territory formation.

Table 1. Glossary of symbols. The first column shows the symbol, the second a definition, and the third whether it pertains to the discrete (lattice) model or the continuous limit or both. Note that some symbols are used either as dimensional quantities or their dimensionless equivalents, depending on the context (see section 2.1.4).

Symbol	Definition	Model
n	Arbitrary lattice site	Discrete
s	Arbitrary time step	Discrete
τ	Length of a single time step	Discrete
l	Lattice spacing	Discrete
$K_i(n,s)$	Probability that n is in agent i's conflict zone (CZ) at time s	Discrete
$\bar{K}_i(n,s)$	Spatially averaged CZ	Discrete
$U_i(n,s)$	The probability that agent i is at site n at time s	Discrete
$\rho_{\tau,l}$	Probability that conflict occurs when agents meet	Discrete
β_l	Rate at which CZ decays due to agents visiting without conflict	Discrete
h	Number of lattice sites for spatial averaging	Discrete
d	Perceptual radius of agent	Discrete
q	Strength of tendency to move away from CZ	Discrete
μ	Decay rate of CZ due to finite memory	Both
x and t	Space and time respectively	Continuous
ρ	Rate at which conflicts occur when animals meet	Continuous
β	Rate at which CZ decays due to agents visiting without conflict	Continuous
$k_i(x,t)$	Probability that x is in agent i's conflict zone at time t	Continuous
$\bar{k}_i(x,t)$	Spatially averaged conflict zone	Continuous
$u_i(x,t)$	The probability density of agent i at time t	Continuous
δ	Perceptual radius of agent	Continuous
c	Magnitude of advection	Continuous
D	Diffusion constant	Continuous
L	Width of terrain in 1D model	Continuous
m	Composite parameter $\mu L^2/\rho$	Continuous
a	Composite parameter D/ρ	Continuous
b	Composite parameter $\beta L/\rho$	Continuous
γ	Composite parameter c/D	Continuous

2.1 The 1D model

First we describe the model in discrete space and time, and then take the continuum limit. Let τ be the time between consecutive time-steps and l the lattice spacing. We work on a 1D line lattice.

2.1.1 The conflict zone

Roughly speaking, we wish say that the agent's 'conflict zone' is the place where it has a reasonably high expectation of experiencing a territorial conflict. Conflicts can only happen if agents are in the same place at the same time. So suppose that agents 1 and 2 meet at a lattice site n at time-step s, and that $\rho_{\tau,l}$ is the probability that a conflict occurs during this time-step. Then n becomes part of the conflict zone during this time-step with probability $\rho_{\tau,l}$.

As time passes without conflicts at point n, each agent gradually begins to view the point as being a less dangerous place to venture. This is bolstered by any visits it makes to n that do not result in a conflict. We model this by assuming that during a time-step, the probability of site n being in the conflict zone changes by a factor of either $1 - \mu\tau$ if the agent does not visit n, or $1 - (\mu + \beta_l)\tau$ if the agent does visit n, where $\mu, \beta_l > 0$. Here, μ models the memory decay of a conflict site that it has not visited for some time, whilst β_l models the increase in expected safety incurred by visiting a site and not experiencing a conflict there. In summary, if we let $K_i(n, s)$ be the probability that site n is in the conflict zone of agent i at timestep s, for $i \in \{1, 2\}$, then

$$
K_i(n, s+1) = \begin{cases} 1 - \mu\tau & \text{with probability } \rho_{\tau,l}, \text{ if agents 1 and 2 are at} \\ & \text{site } n \text{ at time-step } s, \\ [1 - (\mu + \beta_l)\tau]K_i(n, s) & \text{in any other situation where agent } i \text{ is at site } n, \\ (1 - \mu\tau)K_i(n, s) & \text{otherwise.} \end{cases}
$$

$$(1)$$

2.1.2 A model of agent movement

As with the conflict zone, we begin by describing the agents' movement in discrete space and time. Each agent has a diffusive (i.e. random walk) aspect to its motion, to account for those aspects of movement within the territory that we are not explicitly modelling, such as foraging. It also has a tendency to move away from areas that are more likely to be part of the conflict zone and towards areas that are less likely to be in the conflict zone, which we model by biasing the random walk accordingly.

As an agent makes its decision to move, it will examine the area in its immediate vicinity, according to its perceptual capabilities. In other words, it makes its decision based on an *average* over certain near-by lattice sites. To be specific, we assume the probability of moving right (resp. left) is determined by averaging the conflict zone over the $2h + 1$ lattice sites centred d lattice sites to the right (resp. left) of its location, where $h \geq 0, d \geq 1$ are integers. Therefore, we define the locally averaged conflict zone as follows

$$\bar{K}_i(n, s|h) = \frac{1}{2h+1} \sum_{n'=n-h}^{n+h} K_i(n', s). \tag{2}$$

We then define the probability, $f_i(n|n', h, d)$, of agent i moving to a lattice site n, given that it was at site n' in the previous time-step, and given values of h and d, to be

$$f_i(n|n', h, d) = \begin{cases} \frac{1}{2}\left[1 + q\bar{K}_i(n'+d, s|h) - q\bar{K}_i(n'-d, s|h)\right] & \text{if } n = n' - 1, \\ \frac{1}{2}\left[1 - q\bar{K}_i(n'+d, s|h) + q\bar{K}_i(n'-d, s|h)\right] & \text{if } n = n' + 1, \\ 0 & \text{otherwise}, \end{cases} \tag{3}$$

where $q \in (0, 1)$ denotes the strength of bias away from the conflict zone.

2.1.3   The continuum limit

One way to analyse the model given in Equations (1) and (3) would be by performing stochastic simulations of the system. To gain mathematical insight, however, it is convenient to take a continuum limit in both space and time. This leads to the following system of partial differential equations (PDEs), defined on an interval $[0, L]$, for $i = 1, 2$ (see Supplementary Appendix A for a derivation)

$$\frac{\partial u_i}{\partial t} = D\frac{\partial^2 u_i}{\partial x^2} + c\frac{\partial}{\partial x}\left[u_i\frac{\partial \bar{k}_i}{\partial x}\right], \tag{4}$$

$$\frac{\partial k_i}{\partial t} = \rho u_1 u_2 (1 - k_i) - k_i(\mu + u_i\beta). \tag{5}$$

Here, $u_i(x, t)$ is the position probability density for agent i at time t, $k_i(x, t)$ is probability that position x is part of the conflict zone at time t, $\rho = \lim_{\tau\to 0}(\rho_{\tau,l}l^2/\tau)$, $\beta = \lim_{l\to 0}(l\beta_l)$, $D = \lim_{l\to 0, \tau\to 0}[l^2/(2\tau)]$, and $c = 4dqD$.

In Equation (4), $\bar{k}_i(x, t)$ is a local average of $k_i(x, t)$, given as follows

$$\bar{k}_i(x, t) = \begin{cases} \frac{1}{\delta + x}\int_{-x}^{\delta} k_i(x + z, t)\mathrm{d}z & \text{if } 0 < x < \delta, \\ \frac{1}{2\delta}\int_{-\delta}^{\delta} k_i(x + z, t)\mathrm{d}z & \text{if } \delta < x < L - \delta, \\ \frac{1}{\delta + L - x}\int_{-\delta}^{L-x} k_i(x + z, t)\mathrm{d}z & \text{if } L - \delta < x < L, \end{cases} \tag{6}$$

where $\delta = \lim_{l\to 0, h\to\infty}(lh)$. This local averaging arises from the biological considerations regarding the animal's perceptual capabilities, described at the start of section 2.1.2. The precise mathematical form emerges from the limiting process given in Supplementary Appendix A.

Finally, we impose the following boundary and integral conditions, respectively (see Sup-

plementary Appendix A for details)

$$\left[D\frac{\partial u_i}{\partial x} + cu_i\frac{\partial \bar{k}_i}{\partial x} \right]\Big|_{x=0} = \left[D\frac{\partial u_i}{\partial x} + cu_i\frac{\partial \bar{k}_i}{\partial x} \right]\Big|_{x=L} = 0, \tag{7}$$

$$\int_0^L u_i(x,t)dx = 1. \tag{8}$$

2.1.4 A dimensionless version of the model

To reduce the number of parameters in the system, we introduce the following dimensionless variables

$$\tilde{x} = \frac{x}{L}, \ \tilde{t} = \frac{tD}{L^2}, \ \tilde{u}_i(\tilde{x},\tilde{t}) = Lu_i(x,t), \ \tilde{k}_i(\tilde{x},\tilde{t}) = k_i(x,t),$$
$$\tilde{\delta} = \frac{\delta}{L}, \ m = \frac{\mu L^2}{\rho}, \ a = \frac{D}{\rho}, \ b = \frac{\beta L}{\rho}, \ \gamma = \frac{c}{D}. \tag{9}$$

Dropping the tildes over the letters to ease notation, we arrive at the following dimensionless system of equations, which will be the object of 1D mathematical analysis in this paper, for $i \in \{1,2\}$

$$a\frac{\partial k_i}{\partial t} = u_1 u_2(1 - k_i) - k_i(m + bu_i), \tag{10}$$

$$\frac{\partial u_i}{\partial t} = \frac{\partial^2 u_i}{\partial x^2} + \gamma\frac{\partial}{\partial x}\left[u_i\frac{\partial \bar{k}_i}{\partial x}\right], \tag{11}$$

$$\left[\frac{\partial u_i}{\partial x} + \gamma u_i\frac{\partial \bar{k}_i}{\partial x}\right]\Big|_{x=0} = \left[\frac{\partial u_i}{\partial x} + \gamma u_i\frac{\partial \bar{k}_i}{\partial x}\right]\Big|_{x=1} = 0, \tag{12}$$

$$\int_0^1 u_i(x,t)dx = 1, \tag{13}$$

where the dimensionless version of $\bar{k}_i(x,t)$ is

$$\bar{k}_i(x,t) = \begin{cases} \frac{1}{\delta+x}\int_{-x}^{\delta} k_i(x+z,t)\mathrm{d}z & \text{if } 0 < x < \delta, \\[2mm] \frac{1}{2\delta}\int_{-\delta}^{\delta} k_i(x+z,t)\mathrm{d}z & \text{if } \delta < x < 1-\delta, \\[2mm] \frac{1}{\delta+1-x}\int_{-\delta}^{L-x} k_i(x+z,t)\mathrm{d}z & \text{if } 1-\delta < x < 1. \end{cases} \tag{14}$$

Unless otherwise stated, all parameter values are assumed to be non-negative.

2.2 The 2D model

In 2D, we perform our analysis using the full, individual-based, stochastic model, to verify that territorial segregation occurs in the version of our model closest to reality. Simulations are performed on a 25×25 square lattice with reflecting boundary conditions, using 4 agents. At each time-step, an agent at lattice site $\mathbf{n}' = (n_1', n_2')$ moves to one of the four adjacent lattice sites with the following probabilities

$$
f_i(\mathbf{n}|\mathbf{n}', h, d) = \begin{cases}
\min\left\{0.5, \max\left[0, \frac{1}{4}\left(1 + q\bar{K}_i(\mathbf{n}' + (d,0), s|h) - q\bar{K}_i(\mathbf{n}' - (d,0), s|h))\right]\right\} & \text{if } \mathbf{n} = \mathbf{n}' - (1,0), \\
\min\left\{0.5, \max\left[0, \frac{1}{4}\left(1 - q\bar{K}_i(\mathbf{n}' + (d,0), s|h) + q\bar{K}_i(\mathbf{n}' - (d,0), s|h))\right]\right\} & \text{if } \mathbf{n} = \mathbf{n}' + (1,0), \\
\min\left\{0.5, \max\left[0, \frac{1}{4}\left(1 + q\bar{K}_i(\mathbf{n}' + (0,d), s|h) - q\bar{K}_i(\mathbf{n}' - (0,d), s|h))\right]\right\} & \text{if } \mathbf{n} = \mathbf{n}' - (0,1), \\
\min\left\{0.5, \max\left[0, \frac{1}{4}\left(1 - q\bar{K}_i(\mathbf{n}' + (0,d), s|h) + q\bar{K}_i(\mathbf{n}' - (0,d), s|h))\right]\right\} & \text{if } \mathbf{n} = \mathbf{n}' + (0,1), \\
0 & \text{otherwise,}
\end{cases}
\tag{15}
$$

where $q > 0$ and d is a positive integer. When $q < 1$, this is the 2D analogue of Equation (3). We extend our model for use when $q \geq 1$ for extra flexibility. Here, $\bar{K}_i(\mathbf{n}, s|h)$ is the 2D analogue of Equation (2), given as follows

$$
\bar{K}_i(n, s|h) = \frac{1}{H} \sum_{|\mathbf{n}' - \mathbf{n}| \leq h} K_i(\mathbf{n}', s),
\tag{16}
$$

where H is the number of elements in the set $\{\mathbf{n}' : |n' - n| \leq h\}$ and $K_i(\mathbf{n}, s)$ is the probability that $\mathbf{n}$ is in the conflict zone of animal i at time-step s. The evolution of $K_i(\mathbf{n}, s)$ is given by

the following iterative equation (see Equation 1 for the 1D version)

$$K_i(\mathbf{n}, s+1) = \begin{cases} 1 - \mu\tau & \text{with probability } \rho_{\tau,l}, \text{ if agents } i \text{ and } j \text{ are at} \\ & \text{site } \mathbf{n} \text{ at time-step } s, \text{ for some } j \neq i, \\ [1 - (\mu + \beta_l)\tau]K_i(\mathbf{n}, s) & \text{in any other situation where agent } i \text{ is at site } \mathbf{n}, \\ (1 - \mu\tau)K_i(\mathbf{n}, s) & \text{otherwise.} \end{cases}$$

$$(17)$$

We begin simulations with $K_i(\mathbf{n}, s) = 0$ for every lattice site $\mathbf{n}$ and place individuals uniformly at random on the lattice grid. We allow $100,000$ time steps "burn-in" for the conflict zones to form, then run the simulations for a further $100,000$ time steps to obtain the agents' utilisation distribution. It turns out that, for the parameter values we tested, running the simulations for longer does not yield qualitatively significant change in the agents' utilisation distribution (Supplementary Figure 3).

3   Model analysis and results

3.1   Linear stability analysis

We use linear stability analysis to ascertain the conditions under which patterns may be expected to form in the 1D system described by Equations (10-13) (see e.g. [24, chapter 2]). Due to the integral conditions (Equation 13), the constant steady state for $u_i(x,t)$ is $u_{i*}(x) = 1$. The constant steady state $k_{i*}(x)$ for $k_i(x,t)$ is calculated by setting Equation (10) to zero so that

$$u_{1*}(x)u_{2*}(x)[1 - k_{i*}(x)] = k_{i*}(x)[m + bu_{i*}(x)]. \tag{18}$$

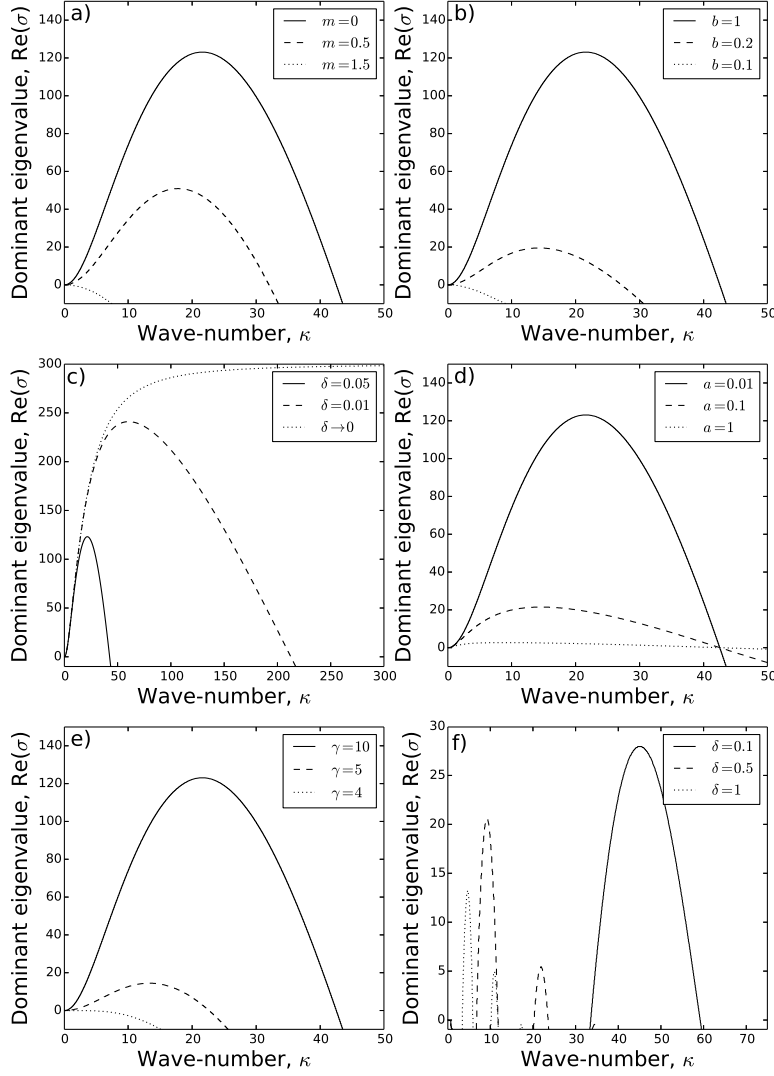Plugging in the constant solution $u_{i*}(x) = 1$ into Equation (18), we find that $k_{1*}(x) = k_{2*}(x) =$

Fig. 1. Dispersion relations. Here we examine the effect of each of the five parameters a, b, γ, δ, m on the dispersion relation for the system of Equations (10-13). For panels (a-e), unless otherwise stated in the figure legend, $a = 0.01$, $b = 1$, $\gamma = 10$, $\delta = 0.05$, $m = 0$. In panel (f) we examine the possibility of pattern formation when $b = 0$. Here, $a = 0.1$, $m = 0.1$, $\gamma = 100$, and δ varies according to the figure legend. See Supplementary Appendix B for an explanation of this choice of parameter values.

k_c, where

$$k_c = \frac{1}{m+b+1}. \tag{19}$$

To linearise about this steady state, we define

$$\mathbf{w} = (\hat{u_1}, \hat{u_2}, \hat{k_1}, \hat{k_2}) = (u_1 - 1, u_2 - 1, k_1 - k_c, k_2 - k_c). \tag{20}$$

We look for solutions of the form $\mathbf{w} = (u_{1,0}, u_{2,0}, k_{1,0}, k_{2,0}) \exp(\sigma t + i\kappa x)$. Then Equations (10-11) imply the following linearised system of equations (as is standard, see e.g. [24, chapter 2])

$$A\mathbf{w} = \sigma\mathbf{w} \tag{21}$$

$$A = \begin{pmatrix} -\kappa^2 & 0 & -\frac{\gamma\kappa}{\delta}\sin(\kappa\delta) & 0 \\ 0 & -\kappa^2 & 0 & -\frac{\gamma\kappa}{\delta}\sin(\kappa\delta) \\ \frac{m}{(m+b+1)a} & \frac{m+b}{(m+b+1)a} & -\frac{m+b+1}{a} & 0 \\ \frac{m+b}{(m+b+1)a} & \frac{m}{(m+b+1)a} & 0 & -\frac{m+b+1}{a} \end{pmatrix}. \tag{22}$$

To determine whether patterns form in this system, we examine the dispersion relation. This plots the largest real value of σ as a function of the wave-number κ, whenever $\det(A - \sigma I) = 0$. If the set of κ-values for which the curve lies above the axis is non-empty then patterns may form with period $2\pi/\kappa$ from small perturbations of the constant steady-state, for any κ in this set. Figure 1 shows the dispersion relation for various values of the parameter space $(a, b, \gamma, \delta, m)$. Though this five-dimensional space is too large to study exhaustively, we can ascertain certain general properties by varying one parameter at a time.

Figures 1a and 1b examine the effects of varying two aspects of the conflict zones decay: that which is proportional to the positional probability of the agent (b) and that which is not (m). If either m is too high or b is too low then patterns cannot form. Therefore the

Table 2. Parameter combinations from Figure 2. The first column gives a phrase explaining each panel in Figures 2a-f, the second states the panel label, and the others give the parameter values used in each panel.

Case	Panel	δ	γ	m	b	a
Base case	(a)	0.05	10	0	1	0.01
Increased spatial averaging	(b)	0.1	10	0	1	0.01
Less advection	(c)	0.05	5	0	1	0.01
Higher memory decay rate	(d)	0.05	10	0.5	1	0.01
Reduced safety from re-visits	(e)	0.05	10	0	0.2	0.01
Greater diffusion/conflict-rate ratio	(f)	0.05	10	0	1	0.1

agent must have some process whereby they feel safer in places they have visited and not had territorial conflicts, so are less likely to view those places as part of the conflict zone. Moreover, this process must be relatively strong compared to the agent's tendency to forget about places they have not visited for a while. In Supplementary Appendix B, we show that if $b = 0$ then territories cannot form for *biologically realistic* parameter values. Nonetheless, there are parameter values where we observe pattern formation and some these are explored in figure 1f (see also Supplementary Appendix C).

Figure 1c shows that as δ is decreased, the set of wavenumbers at which patterns may form increases in size. At the limit $\delta \to 0$, where agents only react to the conflict zone at the precise position they are located, patterns can form at arbitrarily high wavenumbers, so the problem is ill-posed. Therefore it is necessary for territorial formation (in our model) that agents have a non-vanishing perceptive radius which they use to make movement decisions. Similar conditions were discovered in the studies of [25] and [26], regarding territorial scent-marking processes in canid populations.

From Figure 1d, we see that the parameter a, measuring the relative effect of the agent's diffusion constant compared with the rate at which conflicts occur, appears to have no effect on the set of wavenumbers for which patterns form. However, the rate of growth of the resulting patterns is higher when a is lower. Lastly, Figure 1e shows that patterns will only form if γ, the ratio of the advection rate (away from the conflict zone) to the diffusion rate, is sufficiently high.
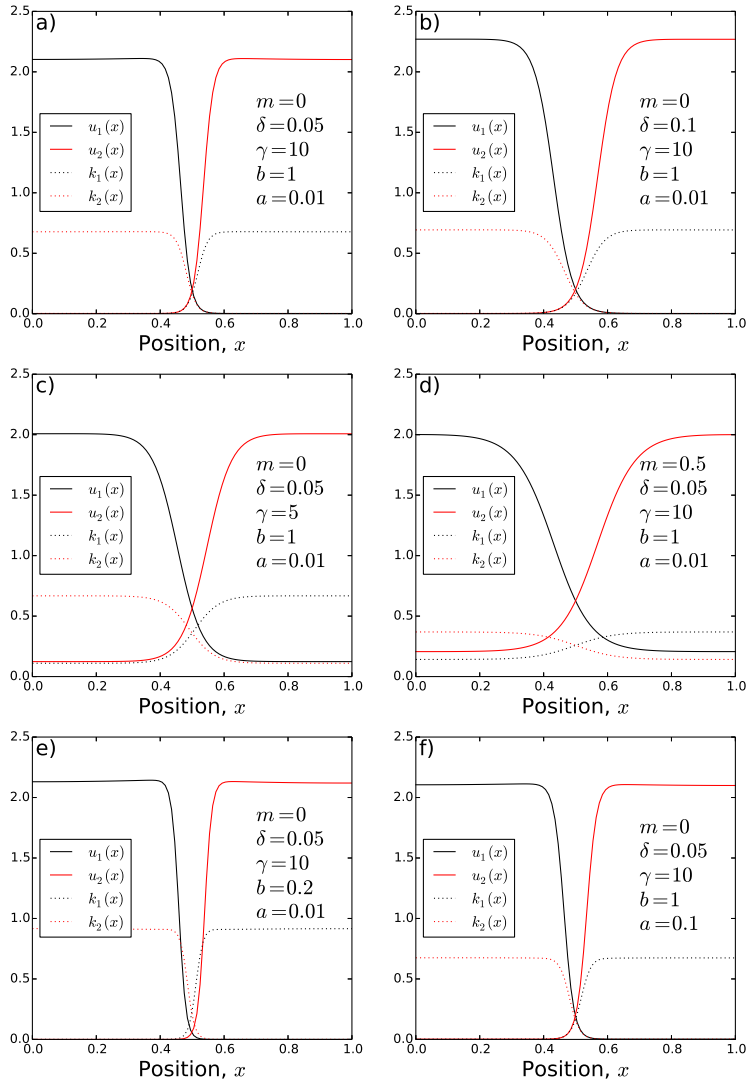
Fig. 2. Numerical solutions corresponding to territories. Here, numerical steady-state solutions to Equations (10-13) are plotted. The respective parameter values are shown in the legends. Panel (a) can be considered as a base case, for comparison with panels (b), (c), (d), (e), and (f), which show the effect on territorial patterns of varying parameters δ, γ, m, b, and a respectively (also see Table 2).

3.2 Numerical analysis: patterns corresponding to territories

Having shown that patterns should form for certain choices of parameter values, we investigate whether the sort of patterns that correspond to territories may form in our system. Such patterns should result in $u_1(x)$ being predominantly concentrated on one side of the interval $[0, 1]$ with $u_2(x)$ on the other side. The steady state of Equations (10-13) is a system of (ordinary) integro-differential equations that is too complicated for exact mathematical analysis. [That this is a system of *integro*-differential equations can be seen by expanding the $\bar{k}_i$ term in Equation (11) using Equation (14).] Therefore we analyse this system numerically, using the method of false transients [27]. Details of the algorithm are in Supplementary Appendix D.

Numerical analysis reveals that patterns can form that look qualitatively like territories for certain parameter values (Figure 2). This analysis allows us to observe the qualitative effects of varying various parameters. By comparing Figure 2a with 2b, we see that a lower perceptual range (δ) of the agent results in sharper territorial boundaries. Figure 2c shows that a lower drift tendency (γ) away from the conflict zone leads to less well-defined territories, with the position density being above about 0.1 across the whole range of the terrain (as compared with Figure 2a where the drift tendency is higher). Similarly, comparing Figures 2d and 2a shows that a tendency for the agents to forget about conflicts in areas they have not recently visited ($m > 0$) leads to less well-defined territories.

Comparing Figures 2e and 2a, we see that lowering b, the tendency for animals to feel safer in areas that they have recently visited and not had a conflict, leads to steeper sides of the conflict zone, and a reduced overall population density (i.e. lower $u_1(x) + u_2(x)$) in the centre of the territory. This reduced population density is analogous to the 'buffer zones' observed in [28], which can give a safe area for prey to exist between territories of predators. Finally, comparing Figure 2f to 2a, we see that changing a (the relative effect of the agent's diffusion constant compared with the rate at which conflicts occur) no effect on the resulting territorial patterns, as one would expect since a vanishes when the left-hand side of Equations (10-11) are set to zero.

3.3 Numerical analysis: transient dynamics

Although steady-state analysis is mathematically convenient, and gives insight into the conditions under which territorial patterns may form, often natural systems are observed in a transient state away from equilibrium [18, 29]. Therefore it is important to examine the profile of the agents' utilisation distributions before they have had time to reach a stable state.

In the system studied here (Equations 10-13), the distributions of both the agents and the conflict zones have an rather interesting trajectory towards the steady state (Figure 3). As the conflict zones emerge, they are initially almost identical in shape (Figure 3a). Then they separate as each agent becomes more familiar with its side of the terrain (Figures 3b and 3c). Eventually, patterns form that look somewhat like territories (Figure 3d), but there is a relatively large probability of being found anywhere on the terrain compared to the eventual steady state. Next, the agents develop a tendency to spend time close to the territory boundary (Figure 3e) causing the borders to sharpen. Once the borders have become sufficiently steep so that intrusion of agent 1 to the right-hand side (or agent 2 to the left-hand side) is very unlikely, the probability density within each territory flattens out to reveal a pattern similar to the eventual steady-state (Figure 3f). It is interesting to note that these varied dynamics occur as an outcome of behavioural rules that are, themselves, fixed through time.

3.4 Mathematical analysis when $\delta \to 0$: an energy method

Though the results of section 3.1 suggest that patterns can form at arbitrary high wavelengths in the limit $\delta \to 0$, in this case the system is simple enough to perform some mathematical analysis. As $\delta \to 0$, the locally-averaged integral $\bar{k}_i$ (Equation 14) tends to k_i, so the system
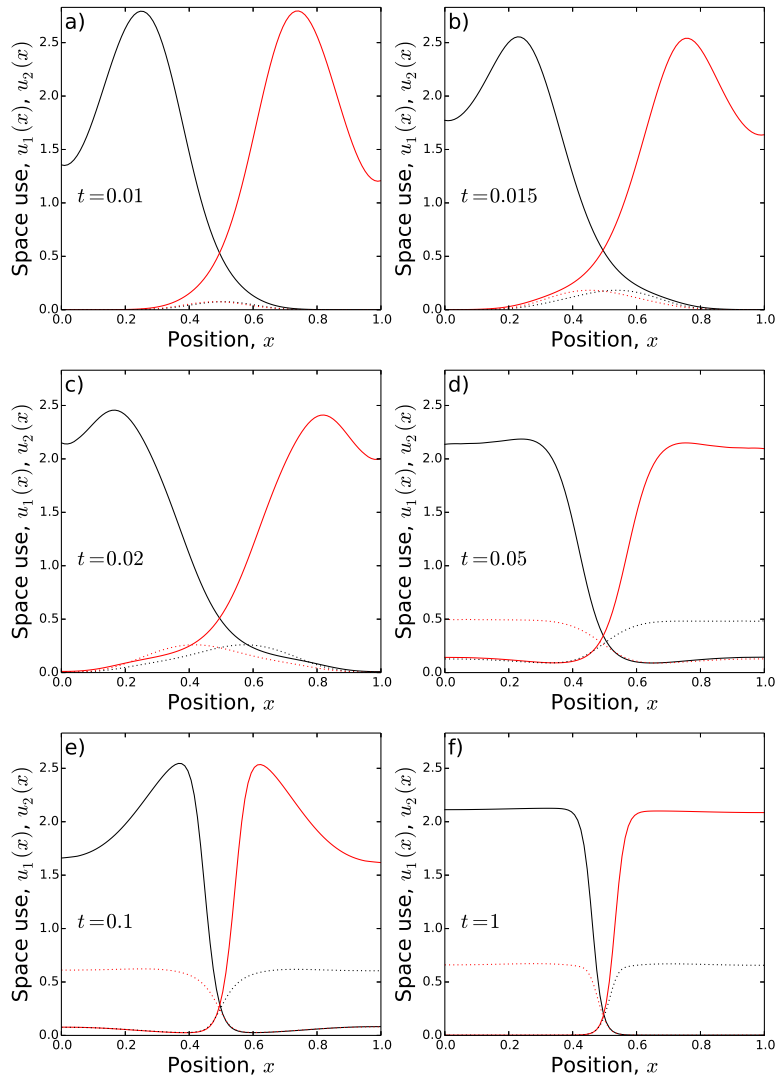
Fig. 3. Transient territorial dynamics. Time-dependent solutions to Equations (10-13) for $a = 0.01$, $b = 1$, $\gamma = 10$, $\delta = 0.05$, and $m = 0$. The value of t is given in each plot, so time increases from panel (a) to (f). Analagous to Figure 2, in each plot $u_1(x, t)$ (resp. $u_2(x, t)$) is given by a red (resp. black) solid curve and $k_1(x, t)$ (resp. $k_2(x, t)$) by a red (resp. black) dashed curve.

from Equations (10-13) becomes

$$a\frac{\partial k_i}{\partial t} = u_1 u_2 (1 - k_i) - k_i(m + bu_i), \tag{23}$$

$$\frac{\partial u_i}{\partial t} = \frac{\partial^2 u_i}{\partial x^2} + \gamma\frac{\partial}{\partial x}\left[u_i\frac{\partial k_i}{\partial x}\right], \tag{24}$$

$$\left[\frac{\partial u_i}{\partial x} + \gamma u_i\frac{\partial k_i}{\partial x}\right]\bigg|_{x=0} = \left[\frac{\partial u_i}{\partial x} + \gamma u_i\frac{\partial k_i}{\partial x}\right]\bigg|_{x=1} = 0, \tag{25}$$

$$\int_0^1 u_i(x,t)dx = 1. \tag{26}$$

Notice that these Equations are identical to Equations (10-13), except that the advection term in Equation (24) contains the function k_i in place of the function $\bar{k}_i$ from Equation (11).

In this section, we analyse the system in Equations (23-26) in the particular case where $a, m = 0$ and $u_1(x,t) + u_2(x,t) = 2$. Notice that $a = 0$ means, in essence, that the conflict zones (k_i) reach equilibrium much faster than the probability distributions of the individuals (u_i). With these assumptions in place, the problem turns out to be simple enough for analysis of the full, time-dependent system, so we can gain some analytic insight into the features we have so far observed by linear analysis and numerics.

Plugging $a, m = 0$ and $u_1(x,t) + u_2(x,t) = 2$ into Equation (23), we can write k_i in terms of u_i as follows, for $i = 1, 2$

$$k_i = \frac{2 - u_i}{b + 2 - u_i}. \tag{27}$$

This means that Equation (24) becomes

$$\frac{\partial u_i}{\partial t} = \frac{\partial}{\partial x}\left[\frac{\partial u_i}{\partial x} + \gamma u_i\frac{\partial}{\partial x}\left(\frac{2 - u_i}{b + 2 - u_i}\right)\right]. \tag{28}$$

A direct calculation shows that Equation (28) is equivalent to

$$\frac{\partial u_i}{\partial t} = \frac{\partial^2}{\partial x^2}\left[\phi(u_i)\right], \tag{29}$$

$$\phi(u_i) = u_i - \gamma b \ln(b + 2 - u_i) - \frac{\gamma b(b+2)}{b + 2 - u_i}. \tag{30}$$

From this, we construct an 'energy' functional

$$E(u_i) = \int_0^1 \Phi(u_i)\mathrm{d}x, \tag{31}$$

where $\Phi(u_i)$ is the anti-derivative of $\phi(u_i)$, i.e.

$$\frac{\mathrm{d}\Phi}{\mathrm{d}u_i}(u_i) = \phi(u_i). \tag{32}$$

The reason for constructing the function $E(u_i)$ is that it turns out to be a decreasing function of time, whose steady-state occurs when the PDE in equation (28) is at steady-state. To see this, observe the following calculation

$$\begin{aligned}
\frac{\mathrm{d}E}{\mathrm{d}t} &= \int_0^1 \frac{\partial}{\partial t}[\Phi(u_i)]\mathrm{d}x \\
&= \int_0^1 \frac{\partial u_i}{\partial t}\phi(u_i)\mathrm{d}x \\
&= \int_0^1 \phi(u_i)\frac{\partial^2}{\partial x^2}[\phi(u_i)]\mathrm{d}x \\
&= \left[\phi(u_i)\frac{\partial \phi}{\partial x}\right]_0^1 - \int_0^1 \left[\frac{\partial \phi}{\partial x}\right]^2 \mathrm{d}x \\
&= -\int_0^1 \left[\frac{\partial \phi}{\partial x}\right]^2 \mathrm{d}x, \tag{33}
\end{aligned}$$

where the third equality comes from Equation (29) and the fifth from the zero-flux boundary conditions (Equation 25).

Notice that the last term in Equation (33) is always non-positive, and is zero precisely when the flux, $-\frac{\partial \phi}{\partial x}$, is zero. Now, if Equation (28) is at steady-state then the flux is constant

across space, say $-\frac{\partial \phi}{\partial x} = C$. However, since the flux is zero at the boundaries ($x = 0, 1$), C must be zero. Thus the flux is zero if and only if Equation (28) is at steady-state. Hence, by (33), $E(u_i)$ decreases over time unless Equation (28) is at steady-state. If the minima of $E(u_i)$ are finite, then $E(u_i)$ is bounded below and so the system will tend towards one of the minima as $t \to \infty$. These minima can therefore be used to describe the eventual state of the system in Equations (23-26). This approach is similar to that of Lyapunov's method for partial differential equations (see e.g. [30]).

For the purposes of this paper, we are particularly interested in minima that correspond to territories. We show in Supplementary Appendix E that when $m = 0$, classical, steady-state solutions to Equations (23-26) must be constant. Hence weak steady-state solutions to Equations (23-26) must be constant except possibly at a set of values with measure zero. As such, solutions that correspond to territories, i.e. with most of the density of the steady-state u_{1*} concentrated on one side and most of the density of u_{2*} on the other side, are such that $u_{1*}(x) = \eta$, $u_{2*}(x) = \zeta$ for $0 \le x < 1/2$ and $u_{1*}(x) = \zeta$, $u_{2*}(x) = \eta$ for $1/2 < x \le 1$.

Furthermore, by the integral condition in Equation (26), we must have $\zeta = 2 - \eta$. It follows that the local minimum energy solutions occur for values of η that minimise the following function, for $0 \le \eta \le 1$

$$\mathcal{E}(\eta) = E(u_{1*}) = \frac{1}{2}\left[\frac{\eta^2}{2} + \gamma b(2b + 4 - \eta)\ln(b + 2 - \eta) - \gamma b(b + 2 - \eta)\right] + \frac{1}{2}\left[\frac{(2-\eta)^2}{2} + \gamma b(2b + 2 + \eta)\ln(b + \eta) - \gamma b(b + \eta)\right]. \tag{34}$$

Since $b \ge 0$ and $0 \le \eta \le 1$, we have $\ln(b + 2 - \eta) > -\infty$ and $\ln(b + \eta) > -\infty$, so that $\mathcal{E}(\eta)$ is finite. Thus $E(u_i)$ is bounded below so the system does, indeed, tend towards a finite-valued minimum.

Analysing Equation (34) numerically for various values of b and γ, we find that minima

occur either when $\eta = 0$ or $\eta = 1$. The minimum $\eta = 0$ gives the following (weak) solution

$$u_{1*}(x) = 0, \quad u_{2*}(x) = 2, \qquad \text{if } 0 \le x < \tfrac{1}{2},$$
$$u_{1*}(x) = 2, \quad u_{2*}(x) = 0, \qquad \text{if } \tfrac{1}{2} < x \le 1, \tag{35}$$

which corresponds to territory formation. The $\eta = 1$ case means that $u_{1*}(x) = u_{2*}(x) = 1$ for all $x \in [0, 1]$, so that territories do not form.

Interestingly, for certain values of b and γ, there are minima at *both* $\eta = 0$ and $\eta = 1$. This is an example of *hysteresis*, where territories only form if the initial conditions are sufficiently close to those in Equation (35), but if initial conditions are close to a constant solution, then territories are not predicted to form. The regions of (b, γ)-space where we see territories, no territories, or both (hysteresis) are shown in Figure 4a.

In Figure 4b, these regions are compared to the regions where linear stability analysis predicts that small perturbations from the constant steady state will grow to non-constant patterns. Despite the various simplifying assumptions made in our energy-functional analysis, the results correspond almost identically to those from linear stability analysis of the full system. Furthermore, they suggest the places where the initial condition can have an effect on the appearance of territorial patterns, and so territories may exist in situations where the constant steady state is stable.

3.5 Simulation analysis in 2D

Figure 5 shows the results of 2D simulation analysis where $\rho = 1$, $\beta = 0.1$ and $\mu = 0$. Notice that by decreasing the parameter q, representing the strength of tendency to retreat, territories have greater overlap (see also Supplementary Figure 4). By decreasing d and h, the scale over which animals make movement decisions, territories become fragmented and less well-defined (see also Supplementary Figure 5). This accords with our observation from 1D linear stability analysis that a lower spatial averaging means the system is susceptible to instabilities at higher
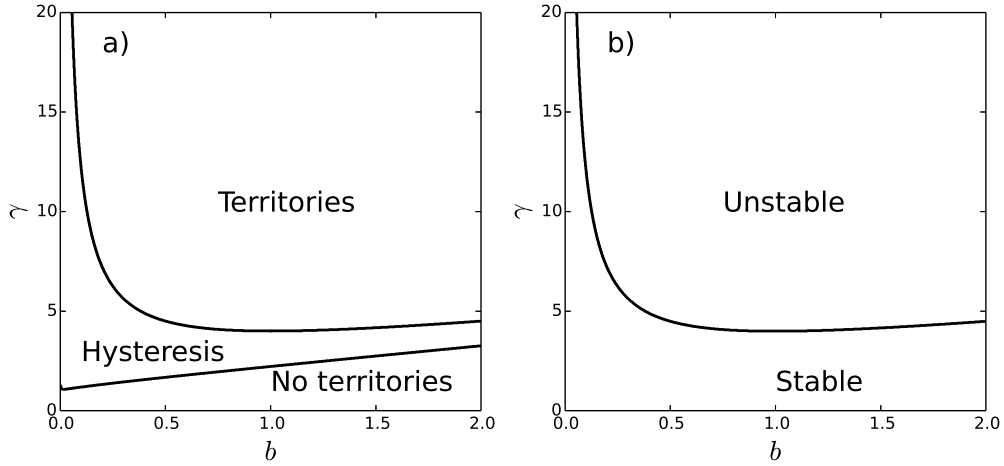
Fig. 4. Predictions of territorial structures. Panel (a) gives the regions of (b, γ)-space where the (non-linear) energy method (Section 3.4) predicts that territories should either form spontaneously (top-right region), decay to the constant steady state (bottom-left), or where the existence of territories depends upon the initial conditions (labelled 'hysteresis'). Here, we assume $a, m = 0$ and $\delta \to 0$. Panel (b) shows the predictions of territory formation from linear analysis of the full system (Equations 10-13). In the 'stable' region, the analysis predicts that territories should not form from small perturbations of the constant steady-state, whereas they may form in the 'unstable' region. In this case, $m = 0$ but the values of a and δ do not affect whether patterns will form for some wave number (see Figure 1c,d).
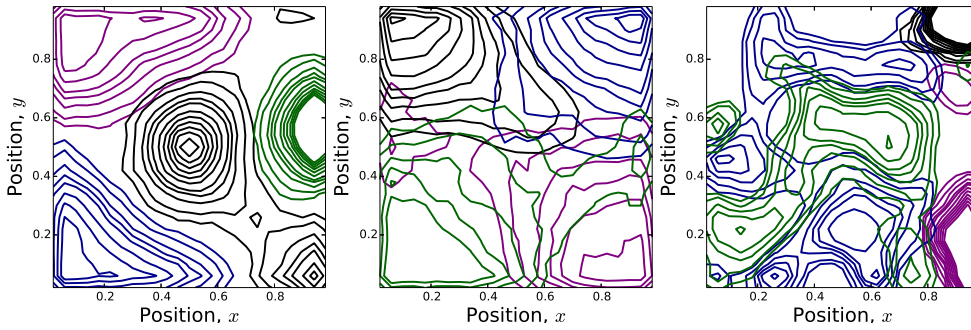

Fig. 5. 2D territories from stochastic IBM. The left-hand panel shows four utilisation distributions that emerge from stochastic simulations when $d = 5$, $h = 5$, $q = 3$. The middle panel shows the effect of reducing the agents' speed of retreat from conflict zones, by reducing q to $q = 2$ and keeping the other parameters constant. The right-hand panel has $d = 2$, $h = 2$, $q = 3$, showing that by reducing the scale over which animals make movement decisions can cause greater territorial fragmentation. Countours are drawn at heights 0.5, 1, 2, 3, 4, 6, 8, 10, 12, 14, 16, from outer to inner.

wavelengths (see Figure 1c).

4   Discussion and conclusions

The aim of this paper is to show mathematically how territorial patterns can form from processes of *direct* interaction between animals. The reason behind studying this is to provide necessary mathematical background for extending the tools of mechanistic home range analysis (MHRA) [13,14] beyond the confines of scent-marking animals, for use with the many species that use direct interactions, such as ritualised aggression, to demarcate territories. We have shown that territories can form from such interactions if the following processes are present

- spatial memory of both past territorial conflicts (encoded in $k_i(x,t)$) and places where such conflicts have not recently occurred (encoded in the parameter b),

- a tendency to move away from places where territorial conflicts have recently occurred,

- a reaction to spatial location averaged over a non-vanishing area centred on the animal.

Recently, spatial memory has been hypothesized as a key process behind many behavioural features in animal populations [31]. This is bolstered by copious studies of neurological 'place cells', which have explained the physiological processes underlying spatial memory in many animals (e.g. [32–34]). Therefore it is reasonable to expect that such memory processes are at play in territorial formation.

Likewise, the other two above-listed process are likely to be typical in most populations of territorial animals. The tendency to move away from the conflict zone is perhaps the most well-established process behind territory formation. For example, [35] defines the process of territorial defence as a "means of repulsion through overt defense or advertisement" and [12] explains how this has become a defining idea in territorial understanding.

The requirement for spatial averaging by an animal deciding where to move is less well-documented, perhaps because it is taken as given that animals make movement decisions based

on their immediate surroundings, not just their exact location. Nonetheless, many continuous-space models make the mathematical simplification that interactions only take place between the animal and its precise current location. This can lead to reasonable results in certain situations [17, 28, 36], but some studies have found that this simplification can dramatically change the nature of observed patters [25, 26]. The results here provide another example of this latter phenomenon.

We also demonstrate the possibility of a *territorial hysteresis* phenomenon occurring in animal populations (e.g. Figure 4). Biologically, this means that animals need to have a certain set of behavioural properties to form territories (encoded in the parameters b and γ), but can relax them slightly once territories have formed and still maintain the territorial structure. Therefore it is possible that animals exhibit slightly different territorial behaviour when forming new territories than in situations where territorial borders have already been established. Such a phenomenon has been observed in a system of scent-marking animals (urban foxes), who respond to changes in territorial structures by altering their scent-marking behaviour [18]. We are, however, unaware of any similar studies regarding animals who perform ritualised aggression to demarcate territories.

The success of MHRA in shedding light on various spatial phenomena in ecology is well documented (see [14] for a recent review). However, its reliance on scent-marking and analogous processes of *indirect* interaction has been a severe limitation until now. The results from this study give the framework to make this extension, by explaining what processes need to be included in a model of territory formation from *direct* interactions. To apply this framework to positional data, one would either fit the steady-state solution of the 2D model to relocation data, using the techniques in [13], or parametrise the model from fine-scale movement, similar to the techniques described in [22]. Since the patterns that arise from direct interactions may be very similar to those from indirect ones, we would generally advocate using the latter, fine-scale techniques (or similar, e.g. [37]). On the scale of behavioural decisions, the difference between the two types of interaction (direct and indirect) is likely to be clearer than on the

scale of long-term territorial patterns.

A programme of research that moves from mathematical analysis to data-driven studies has been successful for understanding scent-marking animals, as evidenced by initial papers containing 1D analysis [28,38] paving the theoretical groundwork for novel insights into real 2D systems [16,17,19]. We have thus followed suit for our study of direct interactions. However, as well as applications to real systems, there is also room for future mathematical investigation of more complicated, multi-agent, 2D systems of direct interactions. Furthermore, the present study assumes that all agents in the system act in the same way, but this is often not true for real animal populations. It would be interesting for future investigations to modify the system to incorporate unequal agents, investigating the varying strategies that may be more or less beneficial for territorial gains, given different behavioural traits. Given the wide range of species that use direct interactions to determine territorial segregation, together with the well-developed statistical techniques for fitting positional data to such models, we hope that the modelling ideas presented here will have broad application to many situations in spatial ecology.

Acknowledgments

Authors' contributions

JRP and MAL jointly conceived, designed, and performed the research. JRP wrote the first draft and MAL contributed substantially to revisions. Both authors have approved the final version of the manuscript.

Competing interests

We have no competing interests.

References

1. King JA. The ecology of aggressive behavior. Annual review of ecology and systematics. 1973;4:117–138.

2. Stamps JA. The Relationship between Resource Competition, Risk, and Aggression in a Tropical Territorial Lizard. Ecology. 1977;58(2):349–358.

3. Kimsey LS. The behaviour of male orchid bees (Apidae, Hymenoptera, Insecta) and the question of leks. Animal Behaviour. 1980;28(4):996 – 1004. Available from: `http://www.sciencedirect.com/science/article/pii/S0003347280800881`.

4. Smith LM, Bertozzi AL, Brantingham PJ, Tita GE, Valasik M. Adaptation of an ecological territorial model to street gang spatial patterns in Los Angeles. Discrete and Continuous Dynamical Systems. 2012;32(9):3223–3244. Available from: `http://aimsciences.org/journals/displayArticlesnew.jsp?paperID=7285`.

5. Gros-Louis J, Perry S, Manson J. Violent coalitionary attacks and intraspecific killing in wild white-faced capuchin monkeys (Cebus capucinus). Primates. 2003;44(4):341–346. Available from: `http://dx.doi.org/10.1007/s10329-003-0050-z`.

6. Sack RD. Human territoriality: its theory and history. vol. 7. CUP Archive; 1986.

7. Gat A. War in human civilization. Oxford University Press; 2006.

8. Maynard-Smith J. Evolution and the theory of games. Cambridge University Press, Cambridge; 1982.

9. Price TD. Sexual selection on body size, territory and plumage variables in a population of Darwin's finches. Evolution. 1984;p. 327–341.

10. Wegge P, Rolstad J. Size and spacing of capercaillie leks in relation to social behavior and habitat. Behavioral Ecology and Sociobiology. 1986;19(6):401–408.

11. Garamszegi LZ, Rosivall B, Hegyi G, Szöllösi E, Török J, Eens M. Determinants of male territorial behavior in a Hungarian collared flycatcher population: plumage traits of residents and challengers. Behavioral Ecology and Sociobiology. 2006;60(5):663–671. Available from: http://dx.doi.org/10.1007/s00265-006-0210-4.

12. Adams ES. Approaches to the Study of Territory Size and Shape. Annual Review of Ecology and Systematics. 2001;32:277–303.

13. Lewis MA, Moorcroft PR. Mechanistic Home Range Analysis. Princeton University Press, Princeton, USA: Princeton University Press; 2006.

14. Potts JR, Lewis MA. How do animal territories form and change? Lessons from 20 years of mechanistic modelling. Proceedings of the Royal Society B: Biological Sciences. 2014;281(1784). Available from: http://rspb.royalsocietypublishing.org/content/281/1784/20140231.abstract.

15. Potts JR, Lewis MA. A Mathematical Approach to Territorial Pattern Formation. The American Mathematical Monthly. 2014;121(9):754–770. Available from: http://www.jstor.org/stable/10.4169/amer.math.monthly.121.09.754.

16. Moorcroft PR, Lewis MA, Crabtree RL. Home range analysis using a mechanistic home range model. Ecology. 1999;80(5):1656–1665.

17. Moorcroft PR, Lewis MA, Crabtree RL. Mechanistic home range models capture spatial patterns and dynamics of coyote territories in Yellowstone. Proceedings of the Royal Society B: Biological Sciences. 2006;273(1594):1651–1659. Available from: http://rspb.royalsocietypublishing.org/content/273/1594/1651.abstract.

18. Potts JR, Harris S, Giuggioli L. Quantifying Behavioral Changes in Territorial Animals Caused by Sudden Population Declines. The American Naturalist. 2013;182(3):E73–E82. Available from: `http://www.jstor.org/stable/10.1086/671260`.

19. Bateman AW, Lewis MA, Gall G, Manser MB, Clutton-Brock TH. Territoriality and home-range dynamics in meerkats, Suricata suricatta: a mechanistic modelling approach. Journal of Animal Ecology. 2015;84(1):260–271. Available from: `http://dx.doi.org/10.1111/1365-2656.12267`.

20. Potts JR, Mokross K, Stouffer PC, Lewis MA. Step selection techniques uncover the environmental predictors of space use patterns in flocks of Amazonian birds. Ecology and Evolution. 2014;4:4578–4588.

21. Kays R, Crofoot MC, Jetz W, Wikelski M. Terrestrial animal tracking as an eye on life and planet. Science. 2015;348(6240).

22. Potts JR, Mokross K, Lewis MA. A unifying framework for quantifying the nature of animal interactions. Journal of The Royal Society Interface. 2014;11(96):20140333.

23. Jullien M, Thiollay JM. Multi-Species Territoriality and Dynamic of Neotropical Forest Understorey Bird Flocks. Journal of Animal Ecology. 1998;67(2):227–252.

24. Murray JD. Mathematical Biology II: Spatial Models and Biomedical Applications. Interdisciplinary Applied Mathematics. Springer New York; 2011. Available from: `https://books.google.co.uk/books?id=2d-RLuD_MX8C`.

25. Briscoe B, Lewis M, Parrish S. Home range formation in wolves due to scent marking. Bulletin of Mathematical Biology. 2002;64(2):261–284. Available from: `http://dx.doi.org/10.1006/bulm.2001.0273`.

26. Potts JR, Lewis MA. Territorial pattern formation in the absence of an attractive potential. Journal of Mathematical Biology. 2015;72(1):25–46. Available from: `http://dx.doi.org/10.1007/s00285-015-0881-4`.

27. Mallinson GD, de Vahl Davis G. The method of the false transient for the solution of coupled elliptic equations. Journal of Computational Physics. 1973;12(4):435 – 461. Available from: `http://www.sciencedirect.com/science/article/pii/0021999173900971`.

28. Lewis MA, Murray JD. Modelling territoriality and wolf-deer interactions. Nature. 1993;366:738–740.

29. Tao Y. On Movement Ecology: A Study of Dynamics. University of California, Davis; 2014.

30. Hsu SB. A survey of constructing Lyapunov functions for mathematical models in population biology. Taiwanese Journal of Mathematics. 2005;9(2):pp–151.

31. Fagan WF, Lewis MA, Auger-Méthé M, Avgar T, Benhamou S, Breed G, et al. Spatial memory and animal movement. Ecology Letters. 2013;16(10):1316–1329. Available from: `http://dx.doi.org/10.1111/ele.12165`.

32. O'Keefe J, Dostrovsky J. The hippocampus as a spatial map. Preliminary evidence from unit activity in the freely-moving rat. Brain research. 1971;34(1):171–175.

33. Langston RF, Ainge JA, Couey JJ, Canto CB, Bjerknes TL, Witter MP, et al. Development of the spatial representation system in the rat. Science. 2010;328(5985):1576–1580.

34. Killian NJ, Jutras MJ, Buffalo EA. A map of visual space in the primate entorhinal cortex. Nature. 2012;491(7426):761–764.

35. Wilson EO. Sociobiology: The New Synthesis. Belknap Press of Harvard University Press; 2000. Available from: `https://books.google.co.uk/books?id=v7lV9tz8fXAC`.

36. Moorcroft PR, Barnett AH. Mechanistic home range models and resource selection analysis: a reconciliation and unification. Ecology. 2008;89:1112–1119.

37. Niu M, Blackwell PG, Skarin A. Modeling interdependent animal movement in continuous time. Biometrics. 2016;.

38. Lewis MA, White KAJ, Murray JD. Analysis of a model for wolf territories. Journal of Mathematical Biology. 1997;35(7):749–774. Available from: `http://dx.doi.org/10.1007/s002850050075`.